SIMULATION OF INTRINSIC INCLUSION MOTION AND DISSOLUTION DURING THE VACUUM ARC REMELTING OF NICKEL BASED SUPERALLOYS

W. Zhang, P.D. Lee and M. McLean
Department of Materials, Imperial College
London SW7 2BP, UK

R.J. Siddall
Special Metals Limited, Wiggin Works, Holmer Road
Hereford HR4 9SL, UK

Abstract

Vacuum Arc Remelting (VAR) is one of the state-of-the-art secondary re-melting processes that are now routinely used to improve the homogeneity, purity and defect concentration in modern turbine disc alloys. The last is of particular importance since, as the yield strength of turbine disc alloys has progressively increased to accommodate increasingly stringent design requirements, the fracture of these materials has become sensitive to the presence of ever smaller defects, particularly inclusions. During the manufacture of these alloys extrinsic defects can be introduced in the primary alloy production stage from a variety of sources; these include ceramic particles originating from crucibles, undissolved tungsten (or tungsten carbide) and steel shot. In addition intrinsic inclusions can be produced during the VAR process itself such as those originating from the crown and shelf, often termed 'white spot'. VAR has proven to be effective in controlling inclusion content but optimization of the process, particularly for a new alloy composition, is a difficult and expensive exercise. Therefore, there is considerable interest in the use of numerical models to relate the process control variables to the final microstructure.

A transient macroscopic model of the VAR process has been developed and applied to simulate inclusion motion in the melt pool and the dissolution of these thermodynamically unstable phases in a liquid metal environment. The model has been applied to determine the trajectories, thermal history and dissolution of intrinsic particles for typical melt conditions of INCONEL 718*.

Introduction

The VAR process has been investigated previously by both experimental and mathematical techniques. Early mathematical approaches solved for heat transfer and approximated the fluid flow by using an enhanced thermal conductivity in the molten region [1]. The next stage of modeling complexity incorporated the fluid flow using a quasi-steady state assumption [2,3]. More recently Jardy *et al.* [4] presented a model that simulated the transient growth of the ingot and macrosegregation. In the last few years some authors have used macromodels to investigate how the formation of defects such as freckles correlated to operational parameters [5,6]. The macromodels have also been coupled to micromodels to predict how these operational parameters alter the formation of grains and other microstructural features [7]. Another application of these macroscopic process models is the prediction of inclusion behavior. A preliminary study illustrating how particle tracking could be added to a process model was presented by the current authors [8].

This paper presents an extension of a transient model of the heat, mass and momentum transfer during VAR to include intrinsic particle dissolution. The origins of these particles are described first, followed by the theory of the particle tracking and dissolution model. The model is then applied to predict the thermal history and trajectories of a series of particle sizes,

* INCONEL is a trademark of Special Metals Corporation

Superalloys 2000
Edited by T.M. Pollock, R.D. Kissinger, R.R. Bowman,
K.A. Green, M. McLean, S. Olson, and J.J. Schirra
TMS (The Minerals, Metals & Materials Society), 2000

types and entry locations. The dissolution rate of these particles, and maximum size which can be safely dissolved, are explored.

Inclusion Origins

One of the practical benefits of vacuum arc remelting is its known ability to reduce the number of inclusions introduced in the primary alloy production stage. These extrinsic inclusions can come from a variety of sources including: ceramic particles from agglomerates of oxide and nitride particles; and undissolved tungsten (or tungsten carbide from machining tools). Between primary melting and VAR, steel shot used for cleaning may also become lodged in the outer surface of the electrode or trapped in the VAR crucible, turning into a potential source of inclusions. Finally, during the VAR process itself, intrinsic inclusions can be produced such as those originating from the crown and shelf, often termed 'white spots' because of their lighter etching appearance in billets. In this paper the inclusions will be subdivided by the location from which they originate: the crucible; the electrode; or the outer surface of the electrode.

From the Crucible

Waves or perturbations on the surface of the melt pool and metal vapor transport from the arc plasma can cause an area of rapidly solidified metal to form on the water-cooled crucible above the melt pool in the VAR process. This region is termed the 'shelf' and 'crown'. Oxide and nitride contaminants washed to the outside of the melt can also be entrained in the crown. Perturbations in the system may cause a fragment, especially of the crown, to detach from crucible wall and fall into the melt pool. The fragment may not completely remelt in the pool but instead it may be entrapped in the mushy zone, where it could form an inclusion (white spot), with or without ceramics particles, in the final ingot.

Electrode

Tungsten or tungsten carbide from cutting tools may exist as extrinsic inclusions in the consumable electrode. Although these are heavy particles that might not be efficiently removed or remelted, there was insufficient data on the dissolution rates to simulate these particles properly, and they have been left as a future topic for study. In this paper only intrinsic particles originating from the electrode will be studied, Nb lean electrode fall-in.

Vacuum induction melting (VIM) is used to obtain the correct composition and this liquid metal is then poured into a mold to produce the electrode for VAR. As the electrode solidifies, shrinkage occurs resulting in a pipe cavity towards the top of the electrode. In the shrinkage, dendrites of primary phase are often exposed as the liquid metal is drawn back to feed volumetric shrinkage closer to the mold wall. Some of this forest of large, solute lean dendrites may fall into the VAR melt pool. As the electrode is remelted in the VAR process, the interdendritic material will melt first due to its lower melting point, further exposing the dendrite spines. These dendrites may melt faster near their trunks due to greater heat flow from conduction and the presence of increased solute causing them to fall in before being completely molten. If the dendrites do not completely melt in the pool before being entrapped in the mushy zone, they may cause solute depleted regions.

For some operating conditions a ridge or torus of metal will form at the outer edge of the electrode, thought to be dendrite fragments exposed by preferential melting [9]. This torus is solute lean. If it is undercut, falls into the melt, and survives until trapped in the mushy zone, it could form white spot similar to the 'pipe' dendrite clusters and crown fall-in.

Electrode Outer Surface Fall-in

As already mentioned above, the consumable electrode is produced by casting VIM melted metal into a mold. The metal is poured into the cold mold from a considerable height. When the molten stream of metal hits the bottom of the 2 m mold, it can splash up and freeze high on the wall. As the mold is further filled and the melt level passes above these frozen splashes, enveloping them, but not always completely remelting them. These splash particles may be detached from the electrode surface when heated by a cathode spot climbing up the electrode. If a sufficiently large mass of splash falls into the melt pool, it may not be completely remelted before entrapment in the mushy zone, becoming a region of different composition and microstructure in the final ingot.

Model Description

A transient finite volume model with a moving mesh was used to simulate the VAR ingot formation, solving the momentum, heat transfer and electric potential equations. This model has been presented elsewhere [3,7], hence only the development of particle trajectory and melting/dissolution theory is presented below.

Particle Motion

There are two well established methods of simulating the behavior of particles in molten metal. The first approach assumes a high density of fine particles, allowing the particles to be treated as a transported scalar - a continuum solute whose concentration is related to the particle density [10]. The second approach considers the behavior of a single independent particle in the fluid. Individual particle tracking provides an ideal way to investigate particle trajectories in the fluid and is particularly appropriate to follow the circulation of intrinsic inclusions; hence this approach was used in the present study.

The motion of an individual particle in a liquid is governed by many factors: the drag force; buoyancy; and capillary forces associated with solid-liquid and solid-solid interfacial interactions. Although the interfacial forces are important for particle agglomeration and adhesion, they are assumed to be negligible in this study. The particles were also assumed to be small compared to changes in the flow field allowing the fluid

flow outside the particle boundary layer to be treated as uniform and particle rotation affects to be neglected.

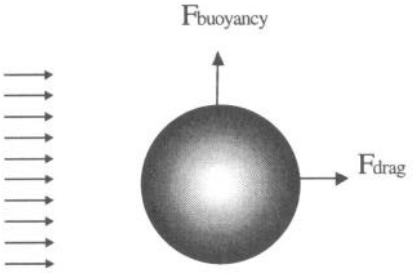

Figure 1. Balance of forces on a particle in a fluid.

With these assumptions the general equation describing particle motion in the fluid can be derived by equating the acceleration of the particle to the buoyancy force, drag force and changes in particle mass, as shown schematically in Figure 1, giving:

$$M_p\left(\frac{d\vec{U}_p}{dt}\right)=V_p(\rho_p-\rho_l)\vec{g} \\ -\tfrac{1}{2}C_D A_p \rho_l\left(\vec{U}_p-\vec{U}_l\right)\left|\vec{U}_p-\vec{U}_l\right|+\frac{dM_p}{dt}\vec{U}_p \quad , \quad 1$$

where M_p is the mass of particle, $\vec{U}_p$ is the velocity of particle, V_p is the volume of particle, ρ_p and ρ_l are the densities of the particle and liquid respectively, C_D is the dimensionless drag coefficient, $\vec{U}_l$ is the fluid velocity, D_p is the particle diameter and A_p is the cross-sectional area of the particle projected on a plane perpendicular to the direction of relative velocity, $\vec{U}_p-\vec{U}_l$. The velocity and properties of the fluid are calculated by interpolation from the macromodel grid. By solving equation 1 for the particle velocity in axial direction, u_p, and radial direction, v_p, the location of particle x_p and y_p can be calculated for each time step.

The drag coefficient, C_D, is calculated as a function of the Particle Reynolds Number, Re_p, as follows [11]:

$$C_D=\begin{cases}24/\mathrm{Re}_p, & 10^{-3}<\mathrm{Re}_p<2\\ 18.5/\mathrm{Re}_p, & 2\le\mathrm{Re}_p\le 500\\ 0.44, & 500<\mathrm{Re}_p\le 2\times10^5\\ 0.09, & 2\times10^5<\mathrm{Re}_p\end{cases}, \quad 2$$

where Re_p is defined as, $\mathrm{Re}_p=\dfrac{\rho_l\left|\vec{U}_p-\vec{U}_l\right|D_p}{\mu}$.

Equation 2 assumes that the particles are spherical and hence is directly applicable only for some intrinsic inclusions. However, many intrinsic inclusions such as crown fall-in and electrode splash are plate-like or disk-like in shape. For non-spherical shapes Heywood [12] has suggested a multiplicative correction factor for the drag force termed the volume shape factor, κ, given by:

$$\kappa=V/d_A^3, \quad 3$$

where V is the volume of particle, d_A is the projected area diameter used to calculate the Re_p and C_D. He found this correlation was suitable for Reynolds numbers in the range of 1 to 1000. For lower Reynolds numbers creeping flow was assumed whilst for higher Reynolds numbers a sphericity correction was applied [13]. For most simulations in this paper Re_p was in the range where equation 3 was applicable.

Particle Melting/Dissolution

The rate at which a particle melts and/or dissolves in the molten nickel based superalloy is dependent upon both the heat and mass transfer between the particle and the surrounding fluid. Some inclusions with high melting points may only be dissolved by solutally driven dissolution; other particles may be dominated by thermally driven remelting. Both of these processes were simulated and are jointly termed 'dissolution' in this paper since they are solved simultaneously. The following assumptions were made in order to simulate the transient dissolution of inclusions during VAR:

1. The heat and mass transport is one dimensional. For spherical particles it is 1D in spherical coordinates; for plate-like particles it is 1D in Cartesian coordinates since the thickness is much smaller than any other dimension.
2. The solute and thermal distributions are uniform around the particle and boundary-layer.
3. The solute concentration at the interface of the film layer and bulk melt is constant, and the temperature of that interface equals that of the surrounding bulk liquid.
4. If a phase change occurs at the liquid and solid interface, thermodynamic equilibrium is established instantly.

With these assumptions, the thermal and solute profiles inside the inclusion are governed by the following partial differential equations. For thermal transport:

$$\frac{\partial(\rho h)}{\partial t}=\frac{1}{r^2}\frac{\partial}{\partial \mathrm{r}}\left(\frac{k}{C_p}\mathrm{r}^2\frac{\partial h}{\partial \mathrm{r}}\right)+S_h, \quad 4$$

Where S_h is a source term accounting for the phase change, ρ is the density, h is the enthalpy, t is the time, k is the thermal conductivity, C_p is the heat capacity and r is the spatial coordinate. For Cartesian coordinates ∂r becomes ∂x and the r^2 and $1/r^2$ terms are set equal to 1.

For solute transport:

$$\frac{\partial(\rho C_i)}{\partial t}=\frac{1}{r^2}\frac{\partial}{\partial \mathrm{r}}\left(D_{i,s}\mathrm{r}^2\frac{\partial C_i}{\partial \mathrm{r}}\right)+S_{C_i}, \quad 5$$

where S_{Ci} is a source term accounting for any reactions, C_i is the concentration of solute i and $D_{i,s}$ is the diffusion coefficient of solute i in the solid particle.

In order to solve these equations the boundary conditions must be determined. These boundary conditions are a strong function of the local flow characteristics, as presented separately below for the thermal and solute models.

Thermal Boundary Conditions and Source Terms The heat transfer between the particle and bulk fluid can be approximated by a heat flux, q_b, dependent upon a solid-liquid heat transfer coefficient, h_{sl}:

$$q_b = A_{sp} h_{sl} (T_{bl} - T_{l\infty}), \quad 6$$

where A_{sp} is the surface area of a particle; T_{bl} is the liquid temperature at the solid/liquid interface which is approximately equal to solid particle surface temperature T_{bs}; and $T_{l\infty}$ is bulk liquid temperature. The solid-liquid heat transfer coefficient is calculated from the Nusselt number, $Nu=h_{sl}D_p/k_l$. Nu is calculated assuming a sphere in forced convection [14]:

$$Nu = 2.0 + 0.6 Re^{\frac{1}{2}} Pr^{\frac{1}{3}}, \quad 7$$

where Pr is the Prandtl number, defined as $Pr = \frac{C_p \mu}{k}$.

Equation 4 is solved in the domain of the solid particle using the boundary condition from equation 6 and a source term to account for the phase change given by:

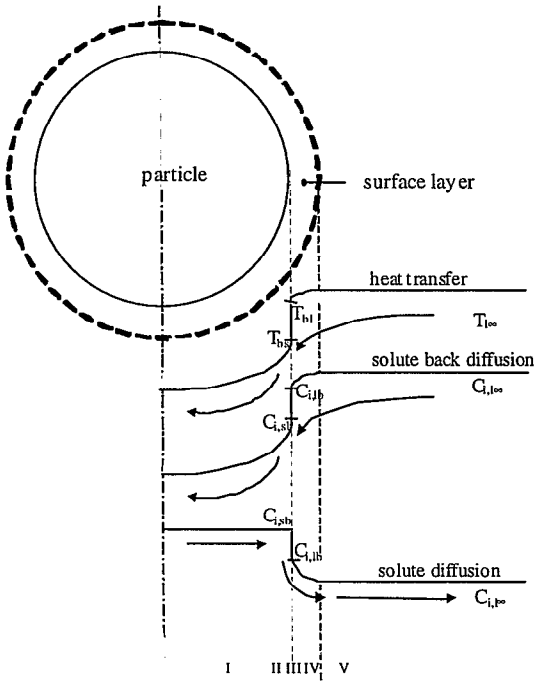

Figure 2. Schematic of particle dissolution mechanisms.

$$S_h = \rho_p L_p \frac{df_s}{dt}, \quad 8$$

where L_p is the latent heat of the particle.

Solute Boundary Conditions and Source Terms The dissolution of a solid particle in a liquid is governed by the rate at which solute molecules on the solid surface leave the face, reducing the mass of particle. The rate at which this process occurs can be controlled by any of the five steps [15,16] shown schematically in Figure 2 and listed below:

I. Solid state diffusion of the solute molecules between particle core and surface.

II. Diffusion across a solid reaction product.

III. Transfer of the solute molecules across the solid-liquid interface to the liquid boundary layer.

IV. Solute diffusion within the liquid boundary layer.

V. Solute transport from the liquid boundary layer through the bulk liquid by a combination of diffusion and convection.

Processes I and II are simulated over the domain of the particle by equation 5 whilst III and V are assumed to be negligible (i.e. there is no kinetic atomic detachment barrier and the bulk liquid is completely mixed). The thickness of solute boundary layer, IV, depends on both the particle properties and fluid properties and can be characterized by the Sherwood number, $Sh_p=h_{i,sl}d_p/D_{i,l}$, which relates an average mass transport coefficient between solute i in the solid and liquid, $h_{i,sl}$, to the molecular diffusivity of solute i in liquid phase, $D_{i,l}$ [17]. Using the mass transport coefficient the boundary condition of solute flux, $f_{i,b}$, for equation 5 can be determined:

$$f_{i,b} = h_{i,sl} A_{sp} (C_{i,l\infty} - C_{i,lb}), \quad 9$$

where $C_{i,lb}$ is solute concentration of liquid at solid/liquid interface; and $C_{i,l\infty}$ is solute concentration of in bulk liquid.

For creeping flow the Sherwood number can be derived from a mass balance equation coupled to the Stokes velocity field [18], obtaining:

$$Sh_p = 1 + (1 + Pe_p)^{\frac{1}{3}}, \quad 10$$

where Pe_p is the Peclet number for a particle, defined as $Pe_p = \frac{|\vec{U}_p - \vec{U}_l| d_p}{D_{i,l}}$. For high Reynolds numbers the empirical correlation given by Clift [17] was used:

$$Sh_p = \begin{cases} 1+\left(1+\frac{1}{Pe_p}\right)^{\frac{1}{3}} Re_p^{0.41} Sc^{\frac{1}{3}}, \\ \quad \text{for } 1 < Re_p \le 100; \\ 1+\left(1+\frac{1}{Pe_p}\right)^{\frac{1}{3}} 0.752 Re_p^{0.472} Sc^{\frac{1}{3}}, \\ \quad \text{for } 100 < Re_p \le 2\times10^3; \\ 1+\left(1+\frac{1}{Pe_p}\right)^{\frac{1}{3}} \left(0.44 Re_p^{\frac{1}{2}} + 0.034 Re_p^{0.71}\right) Sc^{\frac{1}{3}}, \\ \quad \text{for } 2\times10^3 < Re_p \le 10^5. \end{cases} \qquad 11$$

Where Sc is the Schmidt number, defined as $Sc = \frac{\mu}{D_{i,l}}$.

Solution Technique and Simulation Details

In order to simulate the transient dissolution of inclusions in VAR, the thermal and solute profiles inside an inclusion were calculated using an explicit finite volume discretisation of equations 4 and 5 using the boundary conditions and source terms outlined above. A sufficiently small time step was used to ensure many interpolations of the particle motion (equation 1) per macromodel control volume.

The nominal VAR operation parameters used to simulate the macroscopic heat transfer and fluid flow during the INCONEL 718 ingot formation are listed in Table I. The initially quickly changing temperature profile and fluid flow becomes well established after the ingot height reached 0.8 m. Therefore, the thermal and flow field at this stage of the VAR process was used to investigate inclusion behavior.

Table I. Nominal values used to simulate the VAR processing of INCONEL 718.

Parameter	Value	Units
Ingot Diameter	0.510	m
Final Ingot Height	2.00	m
Electrode Diameter	0.435	m
Current	6.3	kA
Volts	23	V
Melt Rate	6.47×10^{-2}	kg/s

In this study particle fall-in from three locations was studied: from the crucible, within the electrode; or on the outer surface of the electrode. Three types of intrinsic particles were considered: spherical; plate shaped; and disk shaped. The thermal physical properties for INCONEL 718 ingot and particle material are listed in Table II. For this study, the particles were assumed to have the same composition as the base material. In reality, the crown material may have an increased level of volatile solutes whilst electrode fall-in may be lean in solute (e.g. Nb). Both of these changes in composition will alter the liquidus and solidus temperatures; however, due to the paucity of experimentally measured compositions, these effects were not included in the model.

Table II. Thermophysical property values for INCONEL 718 (both the melt and intrinsic particles).

Property	INCONEL 718	Units
ρ_l	7050	kg/m^3
ρ_p at 1000 K	7713	kg/m^3
ρ_p at solidus	7500	kg/m^3
ρ_p at liquidus	7050	kg/m^3
$T_{solidus}$	1533	K
$T_{liquidus}$	1609	K
L_p	2.72×10^5	J/kg
C_p	620	J/kg.K
k	25	W/m.K
μ	5.0×10^{-3}	kg/m.s
$D_{Nb,l}$	7.0×10^{-6}	kg/m.s
$D_{Nb,s}$	7.0×10^{-9}	kg/m.s

Results and Discussion

The results are grouped by the source of the particles, beginning with crown fall-in from the crucible. For each source and type of fall-in a sensitivity study was performed to determine how the temperature, size, exact location and height at which the particles drop affect the motion, melt rate and final state (fully melted or entrapped in the mushy zone forming an inclusion). The particle was assumed to become entrapped in the mushy zone once it reached a region with a fraction solid of greater than 0.01. For each set of conditions the maximum size that will fully melt was determined allowing the potential of such inclusions forming to be quantified. The range of conditions was based upon observations in industrial practice with a worst case factor added.

Crucible Fall-in

Fall-in of the crown formed on the crucible is thought to be the greatest source of 'white spot' in VAR ingots. The trajectories of crown fall-in treated as spheres with an initial diameter of 2 mm was simulated using three different initial temperatures, 1233, 1433 and 1533 K. Their predicted trajectories are plotted in Figure 3. All three particles are denser than the melt since they are below the liquidus temperature, hence they are accelerated downwards by gravitational forces. Near the edge of the melt pool a buoyancy driven flow from the top of the melt pool down along the edge of the mushy zone carries the particles down faster, with only the hottest and hence lightest particle escaping entrapment in the solid. The temperature history at the center of each of these three particles is shown in Figure 4. The particle with the highest initial temperature melts completely within 0.23 s, as shown by the particle temperature profile, 0.02, 0.12 and 0.22 s after entering the pool, plotted in Figure 5. Note that for the latter two cases each profile has a constant temperature region - the temperature of the surrounding liquid at that time/location since it has melted completely in this region. The particle with an initial temperature of 1433 K begins to melt but becomes entrapped in the mushy zone after 0.28 s; before it has completely

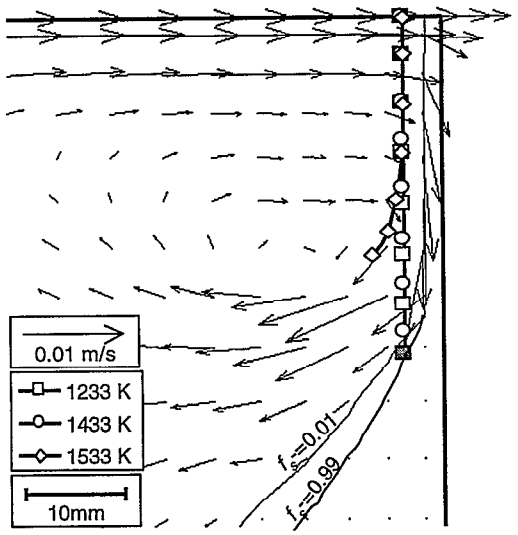

Figure 3. Simulated crown fall-in trajectories for 2 mm diameter spherical particles at three different initial temperatures, 1233, 1433 and 1533 K. (Markers are spaced by 0.04 s.)

melted. The diameter has reduced by 18.5%, a 46% volume reduction. The coldest particle reaches the mushy zone intact - the outer surface has become mushy but is not fully melted.

For all of these simulations and those that follow, it was found that the particle Reynolds number started at approximately 500 and decreased steadily once the particle began to melt. These values for Re_p are well above the creeping flow regime, hence transport across the surface boundary layer dominates the heat and solute transfer between particle and melt.

From an industrial perspective, the important questions are: what is the maximum size of particle that will completely remelt? And, if a particle does not remelt, where will it end up in the ingot? In order to answer these questions, a series of runs was performed on spherically shaped particles altering the size for three initial temperatures, three fall-in heights and three initial radial locations. The maximum size of spherical crown fall-in particles that dissolve completely for the three initial temperatures and three drop heights is shown in Figure 6. Increasing the initial temperature from 1233 K to 1533 K means the particles will melt faster, and are also less dense so that they do not sink as quickly. Therefore, as seen in Figure 6, the maximum size which will be melted increases for a given drop height.

The effect of increasing the drop height for crown fall-in particles from 0 to 30 mm on the maximum diameter that dissolves completely is also shown in Figure 6. The range of heights tested correlates to the industrial observation of melting 20 mm up the electrode plus an extra 10 mm for the arc gap. If the crown particles fall in from just above the melt pool surface, particles whose diameter is less than 3 mm will be safely dissolved if the initial temperature is above 1433 K. The safely dissolved size drops to 2 mm for the 200 K lower

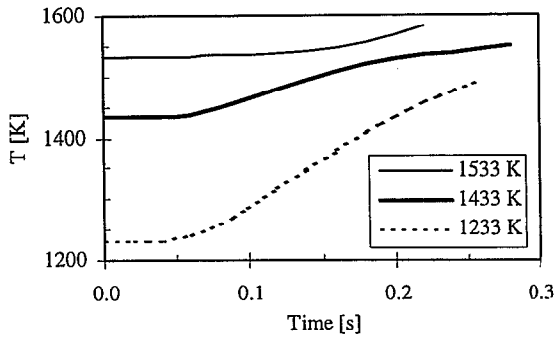

Figure 4. Thermal history at the center of each of the three crown fall-in particles whose trajectory is plotted in Figure 3.

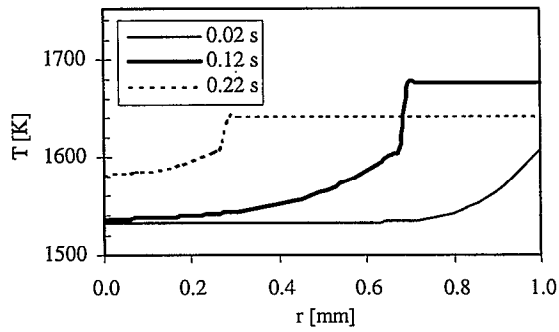

Figure 5. Thermal profile at three different times for the crown fall-in particle with an initial temperature of 1533K whose trajectory is plotted in Figure 3.

initial temperature. When the crown particles drop from 10 mm height, they enter the pool at 0.44 m/s, decreasing the safe diameter to 2.5 mm for an initial temperature of 1533 K; and reducing it further for colder particles or increased heights.

Figure 7 shows the effect of altering the fall-in location from: near the crucible wall (r=250 mm); half way between crucible and electrode (r=236 mm); and near the electrode (r=219 mm). The trend is clear, the nearer the crucible wall, the faster a particle will be trapped in the mushy zone, and hence the smaller the initial safe diameter. The molten metal the particle is exposed to is also colder, further reducing the melt rate.

In summary, the simulations of spherical crown fall-in particles demonstrate that even small (2-3 mm diameter) crown fall in particles may not completely remelt.

Actual crown fall-in particles are more likely to be plate-like rather than spherical, perhaps spreading quite far circumferentially around the mould wall whilst remaining quite thin and close to the surface. Using a plate correction factor for the drag force and one dimensional melting through thickness in Cartesian coordinates, the motion and dissolution of plate-like fall-in was simulated. The maximum thickness for

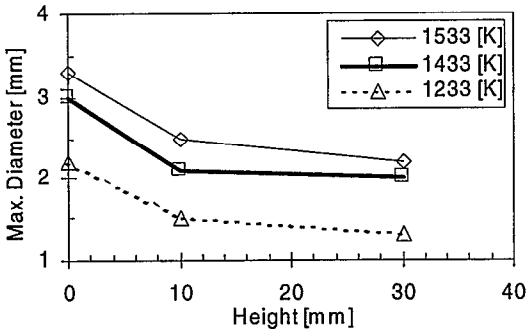

Figure 6. Maximum spherical crown fall-in size that dissolves completely for three initial temperatures and drop heights.

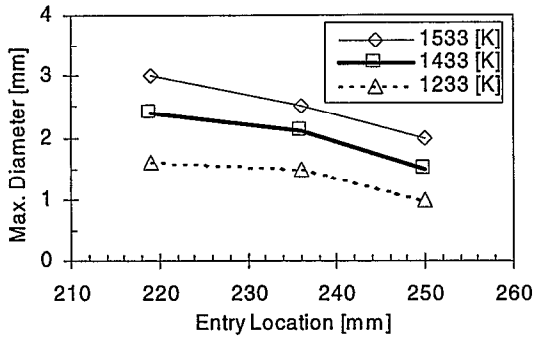

Figure 7. Maximum spherical crown fall-in size that dissolves completely for three different initial locations and temperatures.

complete dissolution of plate-like crown particles sliding into the pool with no initial velocity for three different initial temperatures is given in Figure 8. These results are for a very large plate of dimensions 40 mm long, 20 mm high and of the thickness plotted. For these large plates, the assumption of the particle being small compared to the flow field may be less appropriate, hence the results are approximate. The plate-like structures do not sink as quickly and melt faster than equivalent spheres because the surface area to volume is greater. Even reasonably thick crowns of 4-6 mm, depending on initial temperature, will safely melt.

The maximum safe thickness for different entry locations into the melt pool is shown in Figure 9. Again, as for spherical particles, they are entrapped faster the closer they are to the crucible wall on entering the melt pool. A possible reason for crown fall-in to enter closer to the electrode is if they tip in hinged at the bottom. In which case they may have a velocity component radially inwards, which will increase their residence time in the pool, and hence increase the maximum safe size. The trajectories of 6 mm thick particles as a function of entry location are shown in Figure 10.

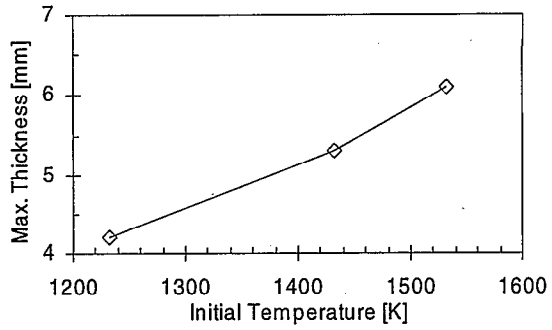

Figure 8. Maximum 40x20 mm plate-like crown fall-in thickness that dissolves completely for three different initial temperatures.

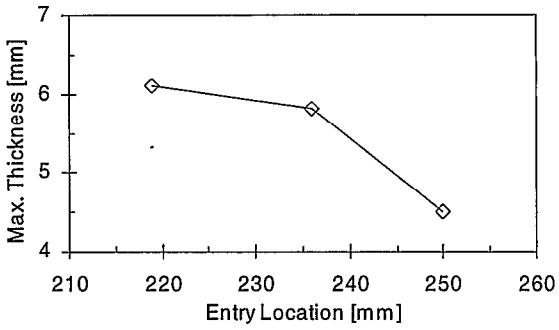

Figure 9. Maximum 40x20 mm plate-like crown fall-in thickness that dissolves completely for three different initial locations.

Electrode Fall-in

In the introduction the different types of particles that might fall-in from the electrode were outlined. A simulation of the trajectories and melting of spherical particles of INCONEL 718 from locations under the electrode allows a comparison with the crucible results. The maximum particle fall-in diameter that dissolves completely for combinations of initial temperatures and drop height are shown in Figure 11. The safe size is much larger than for particles at the outer edge of the pool, due to both higher molten metal temperatures and to greater pool depth. If the particle enters the pool with no initial velocity, superalloy particles or dendrite clusters will melt if the initial diameter is less than 6 mm and the initial temperature is close to the solidus. As the height from which the particles fall from increases the maximum safe size reduces, as expected. If the particles drop from further out the electrode, their chance of survival is greater, as illustrated in Figure 12.

In summary, particles falling in from the pipe in the center of the electrode are more likely to be completely melted than those entering from the crucible wall.

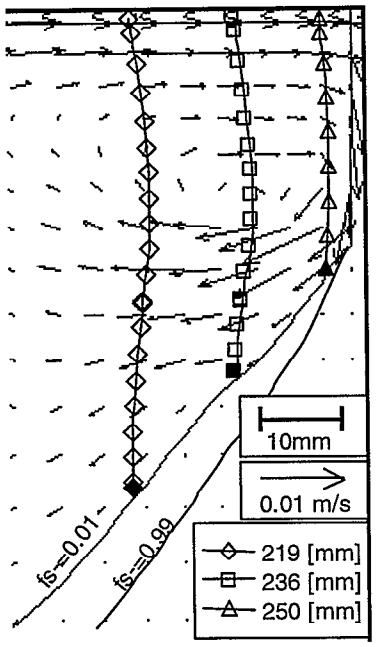

Figure 10. Trajectories of 40x20x5.5 mm plate-like crown fall-in for three different initial radial locations. (Markers are spaced by 0.1 s.)

Electrode Outer Surface Fall-in

The final location for particle fall-in studied was the outer surface of the electrode. In the introduction, the possibility of VIM splash melting off the outside and falling in was discussed. Such pieces of splash were simulated as disk-like shapes, 20 mm in diameter with a thickness of δ. The maximum thickness of such a disk-like splash fall-in that will dissolve completely is plotted in Figure 13 as a function of drop height. Even at the unlikely initial height of 100 mm a 3.5 mm thick disk will melt completely if its initial temperature is near the solidus. Actual pieces of loosely attached splash are unlikely to be very thick due to the way in which they are formed, therefore the simulations would suggest that their potential to be a source of 'white spot' inclusions is low.

For necessary simplicity ideal particle shapes such as spheres, plates and discs have been used for calculations. Also, larger sizes of potential features have been used in the simulations than is likely to be encountered in an industrial furnace to overestimate the potential of entrapment. Both of these assumptions, together with other factors such as increased drag and melting rates for real particles like dendrite fragments, mean the model will under predict the maximum safely dissolving particle size. Much larger fragments will be completely melted than these predictions indicate in an industrial VAR furnace. Therefore, the indicated trends have much relevance in allowing the relative hazards associated with each potential event to be assessed.

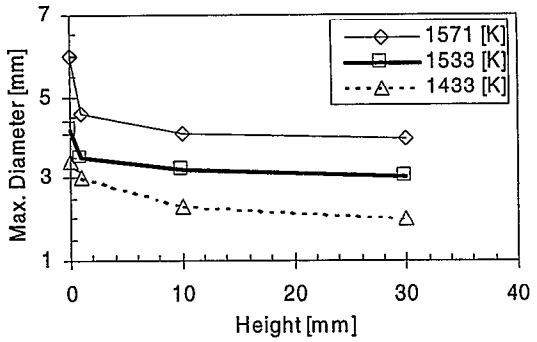

Figure 11. Maximum spherical electrode fall-in size that dissolves completely for three initial temperatures and drop heights.

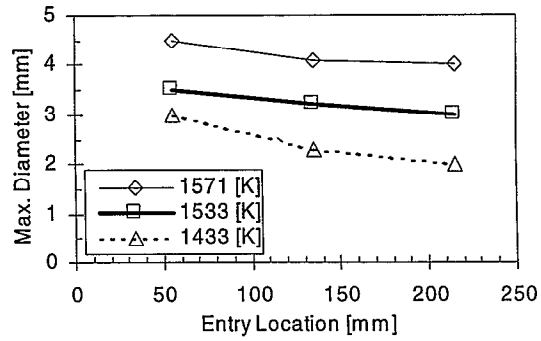

Figure 12. Maximum spherical electrode fall-in size that dissolves completely for three different initial locations and temperatures.

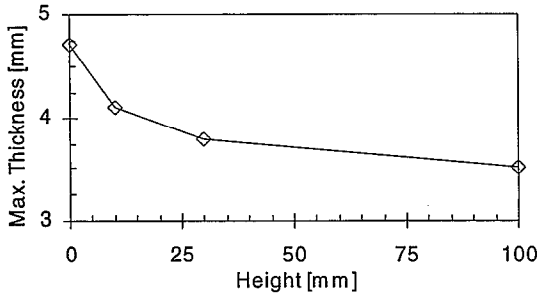

Figure 13. Maximum thickness of a 20 mm diameter disk-like splash fall-in that dissolves completely as a function of drop height.

Summary and Conclusions

A model to simulate the motion, melting and dissolution of particles in the melt pool of the vacuum arc remelting process for the production of INCONEL 718 ingots was developed. The model was used to predict the potential of particles to survive without completely remelting for a range of conditions: entry location; drop height; and particle shape.

Of all the particles studied, crown fall-in from the crucible was found to be the most likely source of 'white spot' inclusions in VAR ingots of INCONEL 718. The maximum safe diameter of spherical fall-in is only 2 to 3 mm if it falls directly in from the crucible wall. If the particles are plate-like instead of spherical, the maximum thickness of crown plate that will completely dissolve is 4 to 6 mm.

Spherical particles falling in from the pipe shrinkage at the center of the electrode were shown to melt completely before entrapment in the mushy zone if the diameter was less than 6 mm. Hence, they form an unlikely source of inclusions in the final ingot.

The detachment of splash from the outer surface of the electrode was also shown to be an unlikely source of inclusions; disk shaped particles up to a thickness of 3 to 6 mm completely remelt before possible entrapment in the mushy zone.

Acknowledgements

The authors would like to thank: Special Metals Wiggin Ltd., Rolls-Royce, DERA, and the EPSRC (GR/L57845 and GR/L86821) for financial support together with the provision of both materials and information. The authors also gratefully acknowledge National Physical Laboratory and the IRC Birmingham for their provision of material property data.

References

1. A.S. Ballantyne and A. Mitchell, "Modelling of Ingot Thermal Fields in Consumable Electrode Remelting Processes", Iron and Steelmaking 2 (1977), 222-239.
2. A. Jardy and D. Ablitzer, "On Convective and Turbulent Heat Transfer in VAR Ingot Pools", Mod. of Casting, Welding and Adv. Sol. Proc. V, Ed. M. Rappaz *et al.*, (TMS 1990) 699-706.
3 P.D. Lee, R.M. Lothian, L.J. Hobbs, and M. McLean, "Coupled Macro–Micro Modelling of the Secondary Melting of Turbine Disc Superalloys", Superalloys 1996, Ed. R.D. Kissinger *et al.*, (TMS 1996) 435-442.
4. A. Jardy, S. Hans and D. Ablitzer, "On the Numerical Prediction of Coupled Transfer and Solidification Process During Vacuum Consumable Arc Remelting of Titanium Alloys", Mod. of Casting, Welding and Adv. Sol. Proc. VII, Ed. M. Cross and J. Campbell, (TMS 1995) 205-212.
5 L.A. Bertram, J.A. Brooks and D.G. Evans, "Transient Melt Rate Effects on Solidification During VAR of 20 Inch Alloy 718", Proc. Int. Sym. Liq. Met. Proc. & Cast., Santa Fe, Feb 21-24, Ed. A. Mitchell, (AVS 1999) 156-167.
6 P. Auburtin and A. Mitchell, "Elements of Determination of a Freckling Criterion", Proc. Int. Sym. Liq. Met. Proc. & Cast., Santa Fe, Feb 21-24, Ed. Mitchell, (AVS 1997) 18.
7 X. Xu, W. Zhang, P.D. Lee and M. McLean, "The Influence of Processing Condition Fluctuations on Defect Formation During VAR of Nickel Based Superalloys", to be published in Proc. Mod. of Casting, Welding and Adv. Sol. Proc. IX, Ed. Sahm *et al.*, (TMS 2000).
8 W. Zhang, P.D. Lee and M. McLean, "Inclusion Behaviour During Vacuum Arc Remelting of Nickel Based Superalloys", to be published in Proc. of EUROMAT 6, Intermetallics and Superalloys, Ed. Morris *et al.*, 27-30 Sept., Munich (1999).
9 J.K Tien and T. Caulfield, Superalloys, Supercomposites and Superceramics, Acad. Press, San Diego, (1989) 80.
10 M.R. Aboutalebi. M. Hasan and R.I.L. Guthrie, "Coupled Turbulent Flow, Heat and Solute Transport in Continuous Casting Processs", Met. Trans. 26B (1995) 731-743.
11 J. Szekely, Fluid Flow Phenomena in Metal Processing, Acad. Press, (1979) 256-257.
12 H. Heywood, Symp. Interact. Fluids Part., Inst. Chem. Eng., London (1962) 1-8.
13 R. Clift, J.R.Grace & M.E. Weber, Bubbles, Drops and Particles, Acad. Press, New York, (1978) 161-162.
14 W.E. Ranz and W.R. Marshall, Jr., Chemical Engineering Progress 48, (1952) 141-146&173-180.
15 Y. Sahai and G.R. St. Pierre, Advances in Transport Process in Metallurgical Systems, Elsevier Sci., (1992) 15.
16 T. K., Sherwood, C. R. Wilke, Mass Transfer, McGraw Hill, N.Y., (1975) 151.
17 R. Clift *et al.*, *ibid*, 117-120.
18 N. P. Cheremisinoff, Handbook of Heat and Mass Transfer Vol. 2, Mass Transfer and Reactor Design, Gulf Pub. Co., Houston, (1986) 59-109.